AIMS Materials Science, 11(1): 102–113.
DOI: 10.3934/matersci.2024006
Received: 05 November 2023
Revised: 23 December 2023
Accepted: 09 January 2024
Published: 17 January 2024

http://www.aimspress.com/journal/Materials

Research article

Employing Na_2CO_3 and NaCl as sources of sodium in $NaFePO_4$ cathode: A comparative study on structure and electrochemical properties

Fahmi Astuti[1], Rima Feisy Azmi[1], Mohammad Arrafi Azhar[1], Fani Rahayu Hidayah Rayanisaputri[1], Muhammad Redo Ramadhan[2], Malik Anjelh Baqiya[1] and Darminto[1,*]

[1] Department of Physics, Faculty of Science and Data Analytics, Institut Teknologi Sepuluh Nopember, Surabaya 60111, Indonesia
[2] Department of Chemical Engineering, Faculty of Industrial Engineering, UPN Veteran Yogyakarta 55281, Indonesia

* **Correspondence:** Email: darminto@physics.its.ac.id.

Abstract: Encouraged by the tremendous success of lithium iron phosphate ($LiFePO_4$), analogous $NaFePO_4$ has been predicted to show identical properties as $LiFePO_4$. Synthesis of $NaFePO_4$ materials in the maricite phase has been carried out using the sol-gel method with variations of calcination temperature and starting materials as sources of sodium Na_2CO_3 and NaCl. The resulted $NaFePO_4$ maricite phase with the purity between 40% and 85%, according to X-ray diffractometry (XRD) characterization was obtained. The morphology and grain size of the particles in samples, as observed by a scanning electron microscope (SEM), tend to enlarge upon calcination at higher temperatures. The increment of calcination temperature increases the $NaFePO_4$ maricite phase content in the sample. The impedance data analysis shows that the diffusion coefficient of Na^+ ions and the electrical conductivity of a sample using Na_2CO_3 is higher than that of NaCl. This comprehensive study provides a feasible method and opens new opportunities for the continuous study of Na-ion batteries.

Keywords: sodium; battery; calcination; morphology; diffusion coefficient

1. Introduction

For the last two decades, the utilization of electronic devices has been an inseparable aspect of everyday life. One of the most important components for electronic devices is the battery, which

provides energy storage and is the main supplier for all electrical energy required for the device's components. Currently, battery commercialization is still limited to the lithium-ion battery (LIB) due to its high-operating voltage and general efficiency. However, the natural supply of lithium is very limited. Even with the discovery of a new lithium deposit in Oregon last month, lithium-shortage is still considered to be the main issue for the development of LIB [1–4]. Based on this, many studies have been conducted to find the alternatives of lithium, in which sodium is one of the most appropriate alternatives due to its large supply in nature and similar characteristics with an LIB when formed into a sodium-ion battery (SIB) [5–11].

In practice, an SIB generates energy by using sodium ions as its charge carrier. However, the main problem for the development of an SIB is its lower cycling capability and weaker structural stability for its cathode material. Aside from those, SIB have similar electrochemical properties to their lithium counterparts. The working voltage of an LIB is 3.4 V, while the working voltage of an SIB is 2.7 V [8]. This difference is not so significant and can be overcome by the addition of dopants [12–15].

$NaFePO_4$ can be classified into two specific structural types (polymorphs): triphylite and maricite. While both structural types have the same anionic framework, the specific crystallographic sites for Na^+ and Fe^{2+} are reversed [16–18]. In 2017, Heubner et al. showed that olivine $NaFePO_4$ can be obtained from the $LiFePO_4$ as a precursor through the delithiation-sodiation method [19]. The cathode material produced through this method showed a specific capacity that was close to the theoretical value of triphylite-type of $NaFePO_4$ (154 mAh g^{-1}) followed by poor cycling ability. The poor cycle characteristic of this sample originated from the different size of Li and Na ion radii, which is aggravated during the Li-Na exchange process to get $NaFePO_4$ from $LiFePO_4$ [20]. Due to the cycle instability and difficulties in the formation of triphylite structure of $NaFePO_4$, the maricite structure of $NaFePO_4$ is the preferred type for cathode material purposes [21,22].

In this study, we report the synthesis of maricite $NaFePO_4$ by employing sol-get method followed by calcination at various air temperatures. The sol-gel method is preferred due to its capability to produce low-impurity maricite $NaFePO_4$. Furthermore, we also investigate the effect of two different sodium sources (NaCl and Na_2CO_3) on the general characteristics of the synthesized $NaFePO_4$. We chose NaCl as the other source of sodium because Indonesia has great potential in sea salt development and production. Aside from the structural analysis of the synthesized sample, an impedance analysis will also be performed to explore the parameters related to the electrochemical properties.

2. Materials and methods

Two $NaFePO_4$ samples were prepared by mixing Na_2CO_3/NaCl, $FeCl_2{\cdot}4H_2O$, and $NH_4H_2PO_4$. The stoichiometric calculation for each material was conducted to produce the exact composition ratio of $NaFePO_4$. For the sol-gel method, the stoichiometric calculations are also conducted for the solvent (HCl/distilled water). For $FeCl_2{\cdot}4H_2O$, $NH_4H_2PO_4$, and NaCl, the chosen solvent is distilled water, while for Na_2CO_3 the chosen solvent is HCl. The chemical reaction of $NaFePO_4$ formation based on NaCl can be explained based on Eqs 1–4:

$$NaCl_{(s)} + H_2O_{(l)} \rightarrow NaCl_{(aq)} \tag{1}$$

$$FeCl_2 \cdot 4H_2O_{(s)} + 2H_2O_{(l)} \rightarrow 2HCl_{(aq)} + Fe(OH)_{2(aq)} + 4H_2O_{(l)} \tag{2}$$

$$NH_4H_2PO_{4(s)} + H_2O_{(l)} \rightarrow NH_4OH_{(aq)} + H_3PO_{4(aq)} \quad (3)$$

$$NaCl_{(aq)} + Fe(OH)_{2(aq)} + H_3PO_{4(aq)} \rightarrow NaFePO_{4(aq)} + HCl_{(l)} + 2H_2O_{(l)} \quad (4)$$

2.1. Thermogravimetric analysis

Thermogravimetric analysis (TGA) was performed by heating the as-synthesized $NaFePO_4$ sample from 27 to 1000 ℃. It can be seen from Figure 1 that the first stage of weight loss (27–150 ℃) of the sample can be attributed to the removal of adsorbed water. The second stage of weight loss (220–330 ℃) is due to the evaporation of CO_2, H_2, and NH_3 that is contained in the precursor materials of $NaFePO_4$. After that, the TGA curve tends to be stable between 400 and 800 ℃. Since the TGA curve shows no indication of further mass reduction up to 840 ℃, the sample was then calcined at 550, 600, and 650 ℃ for 10 h in the air atmosphere.

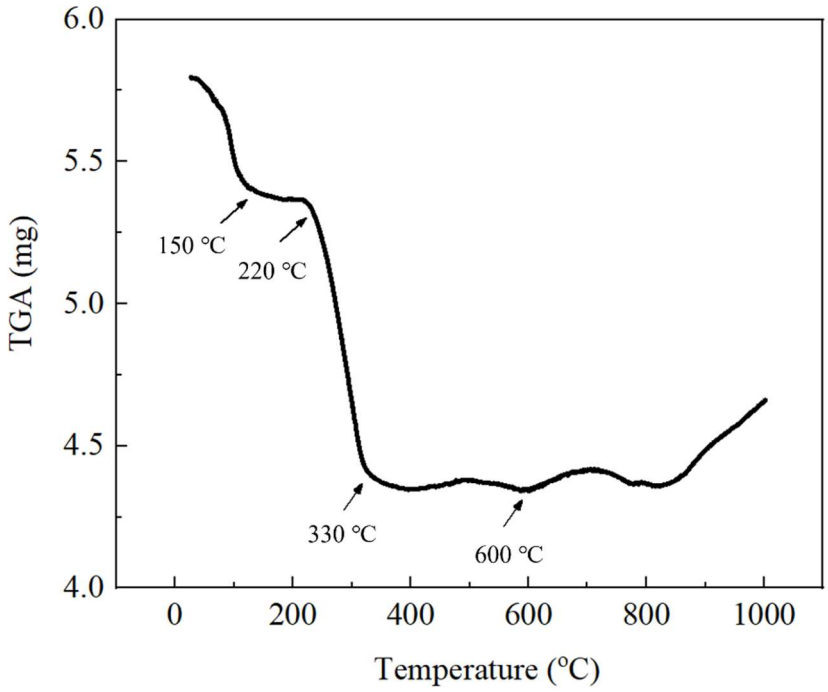

Figure 1. TGA curve for $NaFePO_4$ synthesized using Na_2CO_3 as a sodium source, measured from room temperature to 1000 ℃.

2.2. Structural and electrochemical analysis

All synthesized samples were characterized by X-ray diffractometer (XRD) and scanning electron microscopy that is combined with an energy dispersive X-ray analyzer (SEM-EDAX) to observe the microstructural properties of the sample. The XRD measurement is applied by small angle between $2\theta = 5$ and 60°. The XRD data are obtained by using Cu-Kα radiation $\lambda = 1.54056$ Å with the step data value of 0.04°. To obtain the electrochemical properties of the sample, measurements using electrochemical impedance spectroscopy (EIS) were carried out to determine the ionic and

charge-transfer conductivities as well as ionic diffusivity. In order to determine the electronic conductivity (σ_e), ionic conductivity (σ_i), and the Na^+ diffusion coefficient (D_{Na^+}), we form the half-coin cell from the synthesized sample with NaCl (1M) as the electrolyte component, and all of the aforementioned parameters are analyzed by a Gamry instrument, and the following equations are utilized:

$$\sigma_e = \frac{t}{RctA} \tag{5}$$

$$\sigma_i = \frac{t}{RsA} \tag{6}$$

$$D_{Na^+} = \frac{R^2T^2}{2A^2n^4F^4C^2\sigma^2} \tag{7}$$

where in Eqs 5 and 6, t is thickness (cm) of the sample, *Rct* and *Rs* are charge-transfer and electrolyte resistances (Ω), A is the surface area of the electrode (cm^2). In Eq 7, D_{Na^+} is the diffusion coefficient ($cm^2\ s^{-1}$) of Na^+ ion, R is the ideal gas constant (8.314 J $mol^{-1}K^{-1}$), T is the absolute temperature (298.15 K), n is the number of ions per molecule that move during intercalation process, F is the Faraday constant (96496 C mol^{-1}), C is the concentration of sodium ions in the bulk form, and σ represents the slope.

3. Results and discussion

Parts a and b of Figure 2 show the XRD pattern of the representative samples heat treated in air atmosphere for 10 h using Na_2CO_3 and NaCl, respectively, as sodium sources. Bragg's law (i.e., $2d\sin\theta = n\lambda$) can be applied to investigate the relation between the XRD patterns and the crystal materials, where d, θ, and λ are the spacing in between crystal planes, the incident angle, and the wavelength of the incident X-ray beam, respectively. The qualitative analysis was carried out to identify the maricite phase formation. According to the data base (PDF-98-005-6292), the diffraction peaks of maricite-type $NaFePO_4$ phase are generally observed on all spectra, growing from samples calcined at the lowest to the highest temperatures. Besides, the presence of peaks concerning the impurity phases were also observed. These impurity peaks gradually disappear in the sample that is calcined at higher temperatures. This impurity can be identified as Na-Fe-P-O but has a different stoichiometry than the maricite type ($Na_3Fe_2(PO_4)_3$) with nasicon structure, which is considered an alternative cathode material in sodium-ion batteries that have lower performance and a specific capacity value of 105 mAh g^{-1}, smaller than that of $NaFePO_4$ [23,24]. The presence of $Na_3Fe_2(PO_4)_3$ as an impurity phase in $NaFePO_4$ was also reported by Sun et al. [25]. $NaFePO_4$ is a sample that can easily oxidize, forming the reaction as explained in Eq 8:

$$3NaFePO_4 + \frac{3}{4}O_2 \rightarrow Na_3Fe_2(PO_4)_3 + \frac{1}{2}Fe_2O_3 \tag{8}$$

The purity of $NaFePO_4$ maricite phase using Na_2CO_3 as a sodium source increases along with the calcination temperature. A similar pattern is also observed for XRD data in samples using NaCl as a source of sodium. The sample with the calcination temperature of 650 °C has the lowest impurity. Quantitative calculations of $NaFePO_4$ maricite phase purity based on XRD data for all prepared

samples are summarized in Figure 3. In general, the sol-gel process for oxide compounds followed by calcination in air will inhibit phase formation due to the excess oxygen content.

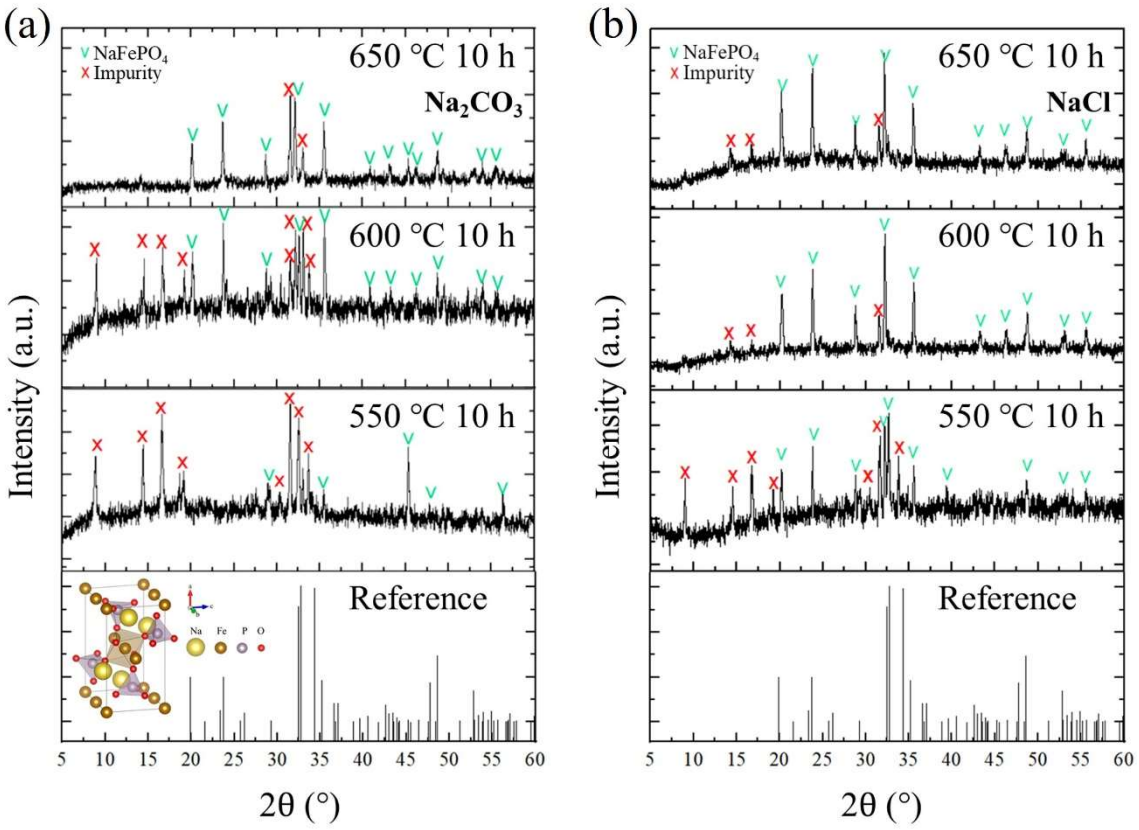

Figure 2. XRD spectra for $NaFePO_4$ powders calcined at various temperatures which used (a) Na_2CO_3 or (b) NaCl as the source of sodium. All diffraction peaks are determined to be the maricite phase or known impurities and are represented by green and red marks, respectively. Inset for (a) shows the crystal structure of maricite phase of $NaFePO_4$.

Scanning electron microscope (SEM) investigation was conducted to provide detailed high-resolution images of the sample by rastering a focused electron beam across the surface and detecting secondary or backscattered electron signals. Through the signal, the information of morphology of the sample can be collected. SEM are also equipped with other detectors that have different analytical capabilities, namely energy-dispersive X-ray spectroscopy (EDX). EDX is a measurement that is used to detect elemental identification and quantitative compositional information. Presented in Figure 4 are the representative micro-structure of the samples calcined in air atmosphere at various temperatures using Na_2CO_3 and NaCl as a source of sodium. It appears that the microstructure develops from initially unclear crystal grains at lower temperature (550 ℃) and evolves to form oval-shaped crystal grains at 650 ℃. There is no abrupt change of morphology of the sample even though the raw material is different. The maricite particles are long-oval shaped, fairly homogeneous, and enlarge upon calcination at higher temperatures. The morphology and averaged grain size of the sample have corroborated the previous synthesis of the same maricite $NaFePO_4$ by solid state reaction [26]. Moreover, the molar ratio of atoms (Na, Fe, P and O) can be estimated from the EDX characterization. The best molar ratio of the constituent atoms Na:Fe:P:O = 1:0.8:0.9:3.7 (closest to 1:1:1:4) is achieved by the sample with

the highest $NaFePO_4$ content. The result of EDX shows that there is no unwanted element, implying that there was no contamination during the synthesis process. As shown in Figure 5, Na, Fe, P, and O peaks are presented in $NaFePO_4$ sample heated at 650 ℃ for 10 h.

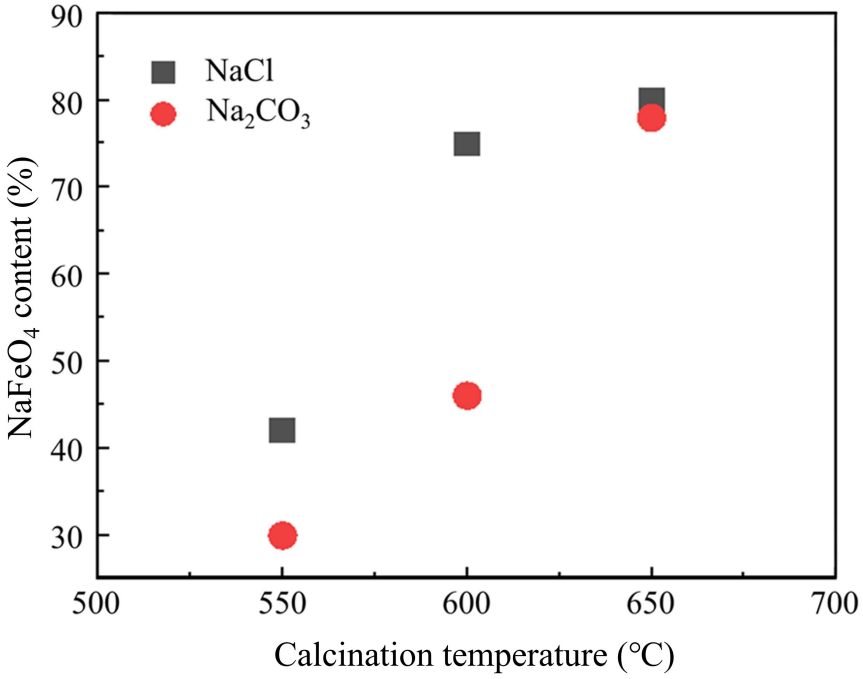

Figure 3. $NaFePO_4$ phase purity percentage with the function of calcination temperature.

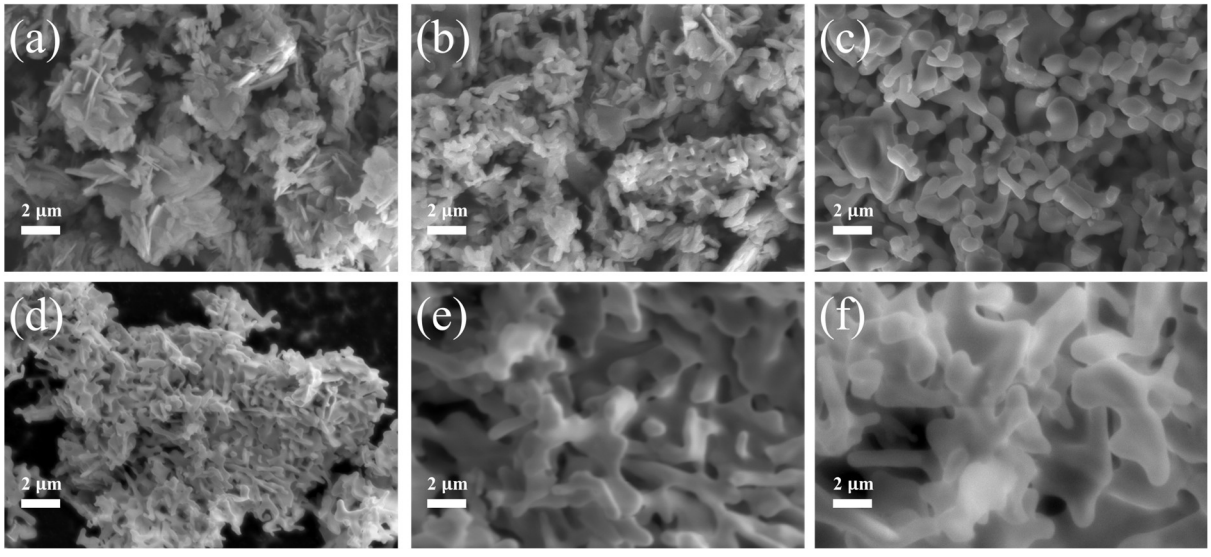

Figure 4. SEM images of $NaFePO_4$ which employs (a–c) Na_2CO_3 and (d–f) NaCl. The calcination temperature variations presented in the figure are (a,d) 550, (b,e) 600 and (c,f) 650 ℃.

As suggested by Yu et al., the lower crystallinity of the sample will reduce the storage performance of battery system. Thus, we only consider the sample that is calcined at 650 °C for 10 h for electrochemical analysis [27]. As given in Figure 6, the Nyquist plot figures the x- and y-axes, standing for the real component (Z') and the imaginary component (Z'') from EIS measurement respectively. The impedance spectrum of a cell in a Nyquist plot consists of two parts: a semicircle (from the diameter, it represents the charge transfer resistance) and a linear tail (from the slope, it reflects the diffusion of Li^+ and Na^+). The semicircle curve in this high frequency region can be determined by the value of *Rs* indicated by the smallest Z' real value and *Rct* which is indicated by the intersection of the semicircle pattern with a straight line. The *Rct* value is related to the charge-transfer resistance, correlating to the electrochemical reaction between the electrode/electrolyte interface. The value of the electrolyte resistance is related to the magnitude of the flow of electron charges in the grain boundary region between particles. The value of *Rs* is related to the electrolyte resistance associated with the movement of Na^+ ions. *Rct* is then used to determine the σ_e, and *Rs* determines the σ_i. The straight line in the low frequency region is also known as the Warburg impedance (Z_w). The Warburg impedance shows the diffusion of sodium ions at the electrode. In the low frequency region, the Warburg coefficient (σ_w) gives the value of the Na^+ diffusion coefficient (D_{Na^+}) [28,29].

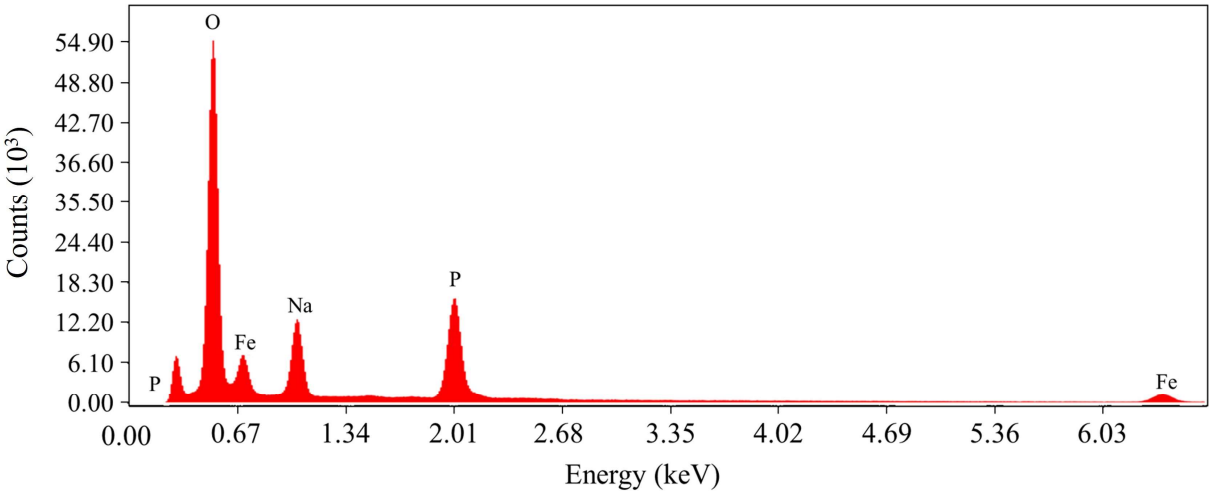

Figure 5. EDAX image of $NaFePO_4$ sample calcined at 650 °C for 10 h. Marked peaks show detected Na, Fe, P, and O.

The Na^+ diffusion coefficient (D_{Na^+}), σ_i, and σ_e are the parameters which can be analyzed from the Nyquist plot. By comparing the semicircle size of Nyquist plot, it is displayed that sample using Na_2CO_3 has higher conductivity rather than NaCl. The ion diffusion of sample using Na_2CO_3 and NaCl are 4.6×10^{-13} and 7.1×10^{-14} $cm^2\ s^{-1}$, respectively. Massaro et al. reported that the sodium ion diffusion value has a scale of $\sim10^{-9}$ $cm^2\ s^{-1}$ calculated by the means of molecular dynamic simulation using a plane polarized force field (Drude model) [30]. Moreover, a study conducted by Liu et al. reported that one of the drawbacks for lithium-ion batteries ($LiFePO_4$) is the sluggish diffusion of lithium ions [31]. They carried out a study related to increasing the diffusion coefficient of Li^+ ions by increasing the concentration of added carbon. In $LiFePO_4$, Li^+ ion diffusion has a scale of $\sim10^{-16}$ $cm^2\ s^{-1}$ without carbon coating and $\sim10^{-13}$ $cm^2\ s^{-1}$ with carbon coating. Therefore, $NaFePO_4$ has an ion diffusion coefficient similar to $LiFePO_4$.

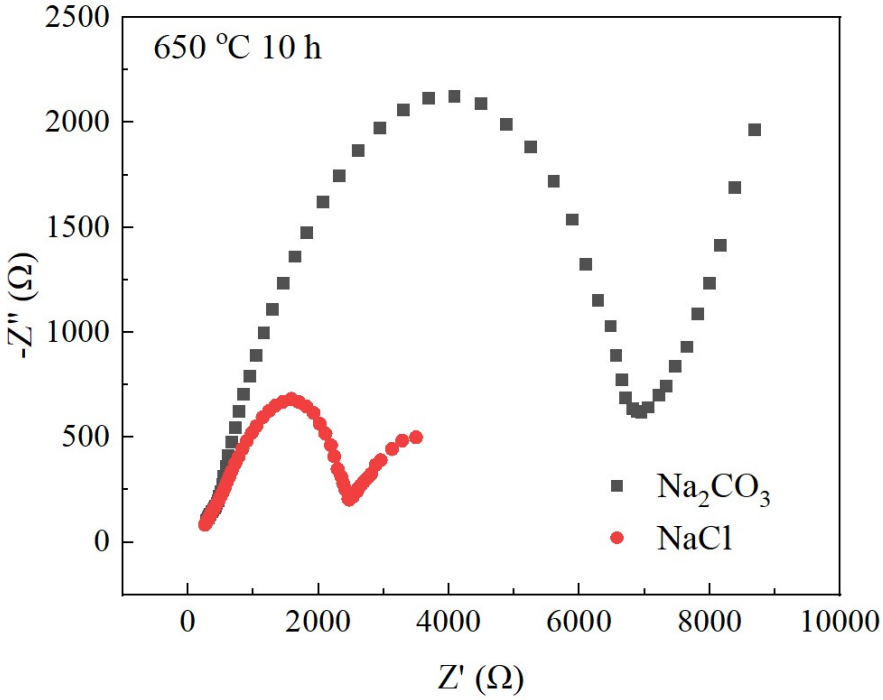

Figure 6. Nyquist plot of $NaFePO_4$ sample calcined at 650 °C for 10 h. The black boxes represent the plot for $NaFePO_4$ with Na_2CO_3 as the sodium source, and the red circles represent the plot for $NaFePO_4$ with NaCl as the sodium source.

The ion diffusion can be studied further using muon spin relaxation (μSR) spectroscopy. Not only for magnetic and superconducting materials [32,33], μSR spectroscopy is also powerful to measure ion diffusion parameters in energy materials [34–36]. In EIS, resistance to ion diffusion through grain boundaries contributes to the total resistance of the sample, increasing the activation energy required for ion conduction, while μSR acts as a local probe, mostly sensing intragrain diffusion for ions [35]. One example of μSR measurement in sodium-ion batteries has been done in a $Na_{1.5}La_{1.5}TeO_6$ system [36]. Using μSR, the sodium-ion diffusion coefficients from the fluctuation rate of muon at different temperatures are expressed using Eq 9:

$$D_{Na^+} = \sum_{i=1}^{n} \frac{1}{N_i} Z_{v,i} S_i^2 v \tag{9}$$

where N_i is the number of accessible sodium sites, $N_{v,i}$ is the vacancy fraction of each destination site, S_i is the distance jumped between sodium ion sites, and v is the hopping rate obtained from μSR data at each temperature. In $Na_{1.5}La_{1.5}TeO_6$ system, sodium ion diffusion coefficient at 300 K of 4.2×10^{-12} cm^2 s^{-1} was achieved by μSR. The diffusion coefficient at room temperature is similar to that reported for the $Na_{0.7}CoO_2$ and $Na_{0.5}CoO_2$ layered cathode materials, which have values of 3.99×10^{-11} and 5×10^{-12} cm^2 s^{-1} respectively [37]. $NaMn_2O_4$ has been reported as a sodium-ion cathode possessing a diffusion coefficient at room temperature of 1.1×10^{-11} cm^2 s^{-1} [38]. The ion diffusion of $Na_{1.5}La_{1.5}TeO_6$ is also comparable with other types of Na^+ ionic conductors, for instance $Na_xWO_2Cl_2$ and Na_3PS_4 with a diffusion coefficient of 10^{-13} and of 10^{-12} cm^2 s^{-1} respectively [39,40]. The ion diffusion of samples in this report are 4.6×10^{-13} and 7.1×10^{-14} cm^2 s^{-1}, which has one order lower than other types of cathodes in sodium-ion batteries mentioned above and several orders lower

compared to the latest experimental result of $NaFePO_4$/C [41]. This could be due to the presence of impurities coming from the $Na_3Fe_2(PO_4)_3$ phase that has lower performance than that of the $NaFePO_4$ phase, since ion diffusion is one of the reasons for the outstanding rate capability. Several studies on diffusion coefficient probing by μSR have been carried out in lithium-ion batteries. The lithium-ion diffusion coefficient in $LiFePO_4$ and $LiNi_{1/3}Co_{1/3}Mn_{1/3}O_2$ at 300 K were reported by μSR to be 3.6×10^{-10} and 3.5×10^{-12} cm^2 s^{-1} respectively [37,42].

Based on the comparison of ion diffusion in lithium-ion and sodium ion batteries, sodium-ions will be a strong candidate for the next generation of battery materials. We show that Na_2CO_3 and NaCl, which have wide availability on Earth, are able to be used as raw materials to obtain $NaFePO_4$ phase that can be employed as cathode battery materials through sol-gel synthesis.

4. Conclusions

The $NaFePO_4$ sample with maricite phase has been successfully synthesized via the sol-gel method, resulting in a phase purity of 80% using either Na_2CO_3 or NaCl as a sodium source. The purity of the synthesized $NaFePO_4$ maricite phase can be achieved even though the sintering process is conducted in ambient atmosphere. Based on SEM characterization, the maricite particles are long-oval shaped and fairly homogeneous, which will be enlarged with increasing calcination temperature. The sodium ion diffusion coefficient of two different sources of sodium have comparable values, indicating a great potential for NaCl to be utilized as an electrode in sodium-ion batteries.

Use of AI tools declaration

The authors declare that they have not used Artificial Intelligence (AI) tools in the creation of this article.

Acknowledgments

The authors would like to acknowledge the funding support from PDUPT research grant No. 923/PKS/ITS/2021 and Penelitian Keilmuan Dana ITS research grant No. 1724/PKS/ITS/2023.

Conflict of interest

The authors declare no conflict of interest.

References

1. Garcia LV, Ho YC, Thant MMM, et al. (2023) Lithium in a sustainable circular economy: A comprehensive review. *Processes* 11: 418. https://doi.org/10.3390/pr11020418
2. Greim P, Solomon A, Breyer C (2020) Assessment of lithium criticality in the global energy transition and addressing policy gaps in transportation. *Nat Commun* 11: 4570. https://doi.org/10.1038/s41467-020-18402-y

3. Liu M, Zhang P, Qu Z, et al. (2019) Conductive carbon nanofiber interpenetrated graphene architecture for ultra-stable sodium ion battery. *Nat Commun* 10: 3917. https://doi.org/10.1038/s41467-019-11925-z
4. Sonoc A, Jeswiet J (2014) A review of lithium supply and demand and a preliminary investigation of a room temperature method to recycle lithium ion batteries to recover lithium and other materials. *Procedia CIRP* 15: 289–293. https://doi.org/10.1016/j.procir.2014.06.006
5. Abraham KM (2020) How comparable are sodium-ion batteries to lithium-ion counterparts? *ACS Energy Lett* 5: 3544–3547. https://doi.org/10.1021/acsenergylett.0c02181
6. Buonomenna MG, Bae J (2017) Sodium-ion batteries: A realistic alternative to lithium-ion batteries? *Nanosci Nanotechnol-Asia* 7: 139–154. https://doi.org/10.2174/2210681206666161019145001
7. Yadav P, Patrike A, Wasnik K, et al. (2023) Strategies and practical approaches for stable and high energy density sodium-ion battery: A step closer to commercialization. *Mater Today Sustain* 22: 100385. https://doi.org/10.1016/j.mtsust.2023.100385
8. Xu G, Amine R, Abouimrane A, et al. (2018) Challenges in developing electrodes, electrolytes, and diagnostics tools to understand and advance sodium-ion batteries. *Adv Energy Mater* 8: 1702403. https://doi.org/10.1002/aenm.201702403
9. Nayak PK, Yang L, Brehm W, et al. (2018) From lithium-ion to sodium-ion batteries: Advantages, challenges, and surprises. *Angew Chem Int Ed* 57: 102–120. https://doi.org/10.1002/anie.201703772
10. Fang Y, Liu Q, Xiao L, et al. (2015) High-performance olivine $NaFePO_4$ microsphere cathode synthesized by aqueous electrochemical displacement method for sodium ion batteries. *ACS Appl Mater Interfaces* 7: 17977–17984. https://doi.org/10.1021/acsami.5b04691
11. Zhao A, Liu C, Ji F, et al. (2023) Revealing the phase evolution in $Na_4Fe_xP_4O_{12+x}$ ($2 \leq x \leq 4$) cathode materials. *ACS Energy Lett* 8: 753–761. https://doi.org/10.1021/acsenergylett.2c02693
12. Clément RJ, Billaud J, Armstrong AR, et al. (2016) Structurally stable Mg-doped P2-$Na_{2/3}Mn_{1-y}Mg_yO_2$ sodium-ion battery cathodes with high rate performance: Insights from electrochemical, NMR and diffraction studies. *Energy Environ Sci* 9: 3240–3251. https://doi.org/10.1039/c6ee01750a
13. Hasa I, Passerini S, Hassoun J (2017) Toward high energy density cathode materials for sodium-ion batteries: Investigating the beneficial effect of aluminum doping on the P2-type structure. *J Mater Chem A* 5: 4467–4477. https://doi.org/10.1039/c6ta08667e
14. Shi Q, Qi R, Feng X, et al. (2022) Niobium-doped layered cathode material for high-power and low-temperature sodium-ion batteries. *Nat Commun* 13: 3205. https://doi.org/10.1038/s41467-022-30942-z
15. Wang J, Fu C, Li Y, et al. (2022) Explore the effect of co doping on P2-$Na_{0.67}MnO_2$ prepared by hydrothermal method as cathode materials for sodium ion batteries. *J Alloys Compd* 918: 165569. https://doi.org/10.1016/j.jallcom.2022.165569
16. Avdeev M, Mohamed Z, Ling CD, et al. (2013) Magnetic structures of $NaFePO_4$ maricite and triphylite polymorphs for sodium-ion batteries. *Inorg Chem* 52: 8685–8693. https://doi.org/10.1021/ic400870x
17. Hwang J, Matsumoto K, Nohira T, et al. (2017) Electrochemical sodiation-desodiation of maricite $NaFePO_4$ in ionic liquid electrolyte. *Electrochemistry* 85: 675–679. https://doi.org/10.5796/electrochemistry.85.675

18. Zheng M, Bai Z, He Y, et al. (2020) Anionic redox processes in maricite- and triphylite-$NaFePO_4$ of sodium-ion batteries. *ACS Omega* 5: 5192–5201. https://doi.org/10.1021/acsomega.9b04213
19. Heubner C, Heiden S, Schneider M, et al. (2017) In-situ preparation and electrochemical characterization of submicron sized $NaFePO_4$ cathode material for sodium-ion batteries. *Electrochim Acta* 233: 78–84. https://doi.org/10.1016/j.electacta.2017.02.107
20. Kundu D, Talaie E, Duffort V, et al. (2015) The emerging chemistry of sodium ion batteries for electrochemical energy Storage. *Angew Chem Int Ed* 54: 3431–3448. https://doi.org/10.1002/anie.201410376
21. Liu H, Li C, Zhang H, et al. (2006) Kinetic study on $LiFePO_4$/C nanocomposites synthesized by solid state technique. *J Power Sources* 159: 717–720. https://doi.org/10.1016/j.jpowsour.2005.10.098
22. Wang D, Wu Y, Lv J, et al. (2019) Carbon encapsulated maricite $NaFePO_4$ nanoparticles as cathode material for sodium-ion batteries. *Colloid Surface A* 583: 123957. https://doi.org/10.1016/j.colsurfa.2019.123957
23. Zhu Y, Xu H, Ma J, et al. (2023) The recent advances of NASICON-$Na_3V_2(PO_4)_3$ cathode materials for sodium-ion batteries. *J Solid State Chem* 317: 123669. https://doi.org/10.1016/j.jssc.2022.123669
24. Xia X, Cao Y, Liu Y, et al. (2019) MCNT-reinforced $Na_3Fe_2(PO_4)_3$ as cathode material for sodium-ion batteries. *Arab J Sci Eng* 45: 143–151. https://doi.org/10.1007/s13369-019-03979-4
25. Sun A, Beck FR, Haynes D, et al. (2012) Synthesis, characterization, and electrochemical studies of chemically synthesized $NaFePO_4$. *Mater Sci Eng B* 177: 1729–1733. https://doi.org/10.1016/j.mseb.2012.08.004
26. Hwang J, Matsumoto K, Nohira T, et al. (2017) Electrochemical sodiation-desodiation of maricite $NaFePO_4$ in ionic liquid electrolyte. *Electrochemistry* 85: 675–679. https://doi.org/10.5796/electrochemistry.85.675
27. Yu F, Wang Y, Guo C, et al. (2022) Spinel $LiMn_2O_4$ cathode materials in wide voltage window: Single-crystalline versus polycrystalline. *Crystals* 12: 317. https://doi.org/10.3390/cryst12030317
28. Kim T, Choi W, Shin H, et al. (2020) Applications of voltammetry in lithium ion battery research. *J Electrochem Sci Technol* 11: 14–25. https://doi.org/10.33961/jecst.2019.00619
29. Ou J, Yang L, Jin F, et al. (2020) High performance of $LiFePO_4$ with nitrogen-doped carbon layers for lithium ion batteries. *Adv Powder Technol* 31: 1220–1228. https://doi.org/10.1016/j.apt.2019.12.044
30. Massaro A, Avila J, Goloviznina K, et al. (2020) Sodium diffusion in ionic liquid-based electrolytes for Na-ion batteries: the effect of polarizable force fields. *Phys Chem Chem Phys* 22: 20114–20122. https://doi.org/10.1039/d0cp02760j
31. Liu H, Li C, Zhang H, et al. (2006) Kinetic study on $LiFePO_4$/C nanocomposites synthesized by solid state technique. *J Power Sources* 159: 717–720. https://doi.org/10.1016/j.jpowsour.2005.10.098
32. Astuti F, Miyajima M, Fukuda T, et al. (2019) Anionogenic magnetism combined with lattice symmetry in alkali-metal superoxide RbO_2. *J Phys Soc Jpn* 88: 043701. https://doi.org/10.7566/jpsj.88.043701
33. Kumar D, Kuo CN, Astuti F, et al. (2018) Nodeless superconductivity in the cage-type superconductor $Sc_5Ru_6Sn_{18}$ with preserved time-reversal symmetry. *J Phys: Condens Matter* 30: 315803. https://doi.org/10.1088/1361-648x/aacf65

34. Månsson M, Nozaki H, Wikberg JM, et al. (2014) Lithium diffusion & magnetism in battery cathode material $Li_xNi_{1/3}CO_{1/3}MN_{1/3}O_2$. *J Phys Conf Ser* 551: 012037. https://doi.org/10.1088/1742-6596/551/1/012037
35. McClelland I, Johnston B, Baker PJ, et al. (2020) Muon spectroscopy for investigating diffusion in energy storage materials. *Annu Rev Mater Res* 50: 371–393. https://doi.org/10.1146/annurev-matsci-110519-110507
36. Amores M, Baker PJ, Cussen EJ, et al. (2018) $Na_{1.5}La_{1.5}TeO_6$: Na^+ conduction in a novel Na-rich double perovskite. *Chem Commun* 54: 10040–10043. https://doi.org/10.1039/c8cc03367f
37. Månsson M, Sugiyama J (2013) Muon-spin relaxation study on Li- and Na-diffusion in solids. *Phys Scripta* 88: 068509. https://doi.org/10.1088/0031-8949/88/06/068509
38. Umegaki I, Nozaki H, Harada M, et al. (2018) Na diffusion in quasi one-dimensional ion conductor $NaMn_2O_4$ observed by μ^+SR. *JPS Conf Proc* 21: 011018. https://doi.org/10.7566/jpscp.21.011018
39. Bruce PG, Nowiński J, Gibson VC (1992) Temperature dependence of sodium ion diffusion in $Na_xWO_2Cl_2$. *Solid State Ionics* 50: 41–45. https://doi.org/10.1016/0167-2738(92)90034-m
40. Zhu Z, Chu I, Deng Z, et al. (2015) Role of Na^+ interstitials and dopants in enhancing the Na^+ conductivity of the cubic Na_3PS_4 superionic conductor. *Chem Mater* 27: 8318–8325. https://doi.org/10.1021/acs.chemmater.5b03656
41. Altundag S, Altin S, Yasar S, et al. (2023) Improved performance of the $NaFePO_4$/hardcarbon sodium-ion full cell. *Vacuum* 210: 111853. https://doi.org/10.1016/j.vacuum.2023.111853
42. Sugiyama J, Nozaki H, Harada M, et al. (2011) Magnetic and diffusive nature of $LiFePO_4$ investigated by muon spin rotation and relaxation. *Phys Rev B* 84: 054430. https://doi.org/10.1103/physrevb.84.054430